

Do Enzymes Stabilize Transition States by Electrostatic Interactions or pK_a Balance: The Case of Triose Phosphate Isomerase (TIM)?

Giuliano Alagona,[†] Caterina Ghio,[†] and Peter A. Kollman^{*,‡}

Contribution from CNR, Istituto di Chimica Quantistica ed Energetica Molecolare, Via Risorgimento 35, I-56126 Pisa, Italy, and Department of Pharmaceutical Chemistry, University of California, San Francisco, California 94143

Received August 8, 1994[⊗]

Abstract: In the triose phosphate isomerase (TIM) catalyzed isomerization of its ligands dihydroxyacetone phosphate (DHAP) and glyceraldehyde phosphate (GAP), it has been established that abstraction of the *pro-R* hydrogen of DHAP by Glu 165 of TIM initiates the reaction to form an enediolate. However, the question whether a proton is transferred (either in a concerted process or subsequently) to the substrate by the electrophilic His 95 has not been definitively established. We present two sets of calculations that bear on this point: First, we show that intramolecular proton transfer of the hydroxyl hydrogen, the enediolate of DHAP, proceeds with a very small barrier. Second, we show that a model for the enediolate has no intrinsic tendency to accept a proton from an imidazole in the presence of the enzyme environment. This disagrees with the interpretation presented by Bash *et al.* (Bash, P. A.; Field, M. J.; Davenport, R. C.; Petsko, G. A.; Ringe, D.; Karplus, M. *Biochemistry* 1991, 30, 5826) in that they argue for His to donate a proton to the enediolate in the TIM mechanism. Our results could, of course, change upon a more accurate representation of DHAP and the enzyme active site. However, they do suggest that the issue of proton transfer to the (incipient) enediolate is still an open one. In addition, these calculations bear directly on the analysis of Gerlt and Gassman (Gerlt, J. A.; Gassman, P. G. *J. Am. Chem. Soc.* 1993, 115, 11552) *vis-à-vis* the putative advantage of an internal pK_a balance in enzyme active sites.

Introduction

The isomerization reaction catalyzed by triose phosphate isomerase (TIM) remains a prototype for the power of enzyme catalysis, with the rate determining step being product dissociation from the enzyme rather than a chemical step.

In a classic set of papers, Knowles and co-workers¹ argued that TIM is a perfectly evolved enzyme. Then, with the advent of site-specific mutagenesis, they “damaged” the enzyme so that the chemical steps were slowed enough to become rate determining. They carried out mechanistic studies on these damaged enzymes to infer what the mechanism of native TIM is, as well as using genetic selection methods to study which further mutations might cause restoration of the full enzymatic activity of native TIM. In the course of those studies, they suggested a new role of His 95 in the enzyme, as a proton donor to make the enediolate of the substrate into an enediol. Evidence for this came from mechanistic studies on native and mutant TIM’s and the considerable loss of catalytic activity upon replacement of His 95 by Gln or Asn.

The fact that TIM might use the imidazole–imidazolate equilibrium to protonate the enediolate has been used by Gerlt and Gassman² as evidence for an “internal pK_a balance” in enzymatic activity. The argument of Gerlt and Gassman is more general than just related to TIM, and it suggests the following question: do enzymes work by electrostatic stabilization of (potentially unstable) ionic intermediates or do they stabilize them by direct protonation or deprotonation? The former

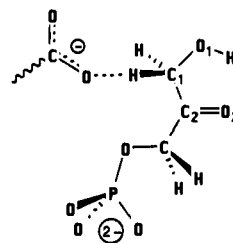


Figure 1. *pro-R* hydrogen abstraction at C₁ of DHAP by Glu 165 (–COO[–]) in TIM.

possibility is certainly the simpler, since it involves fewer chemical steps and a “classic” example of it is the oxyanion hole stabilization in the serine proteases. However, even in the serine proteases, the pK_a of an amide N–H is probably not too different from that of the tetrahedral intermediate. Of course, the question of electrostatic stabilization vs protonation may not have a universal answer and the answer may differ among different enzymes.

Let us now turn to the specific case of TIM. A possible mechanism catalyzed by TIM is given in Scheme 1. The first step in the mechanism is universally accepted as a proton abstraction by Glu 165 of the *pro-R* hydrogen at C₁ of DHAP (Figure 1). As shown by Alagona *et al.*,³ this abstraction would be ~20 kcal/mol uphill for an isolated hydroxy ketone, thus the important roles of His 95, Lys 13, and perhaps Ser 96 and Asn 11 in providing a positive electrostatic potential to make this abstraction facile.

The key question is whether this initial proton abstraction is accompanied by or immediately followed by proton delivery of a proton from His 95 or some other proton donor to form an

[†] Istituto di Chimica Quantistica ed Energetica Molecolare.

[‡] University of California.

[⊗] Abstract published in *Advance ACS Abstracts*, September 1, 1995.

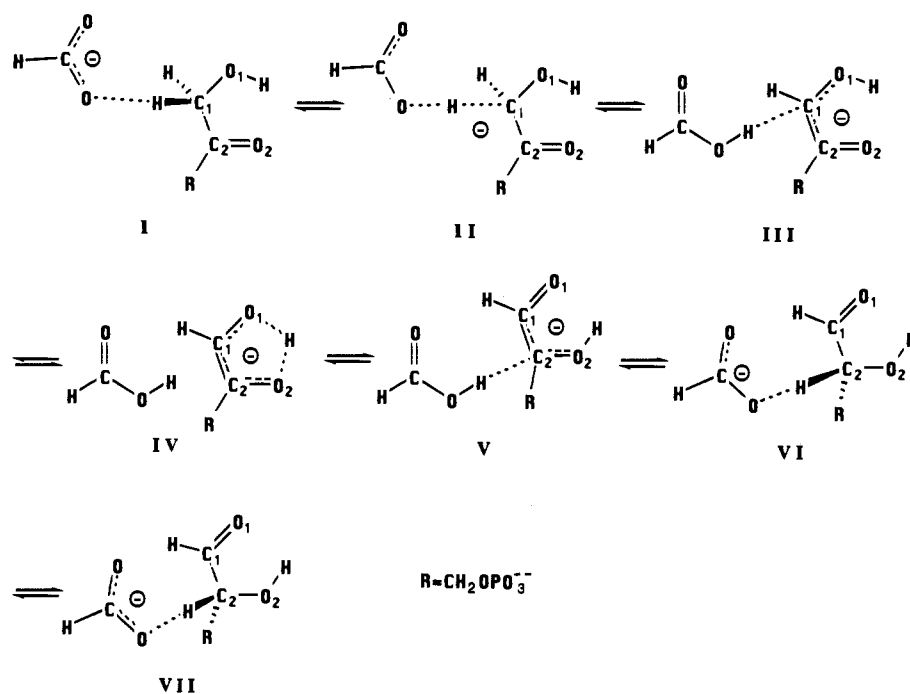
(1) Albery, W. J.; Knowles, J. R. *Biochemistry* 1976, 15, 5588. (b) Leadlay, P. F.; Albery, W. J.; Knowles, J. R. *Biochemistry* 1976, 15, 5617.

(c) Albery, W. J.; Knowles, J. R. *Biochemistry* 1976, 15, 5627.

(2) Gerlt, J. A.; Gassman, P. G. *J. Am. Chem. Soc.* 1993, 115, 11552.

(3) Alagona, G.; Desmeules, P.; Ghio, C.; Kollman, P. A. *J. Am. Chem. Soc.* 1984, 106, 3623.

Scheme 1

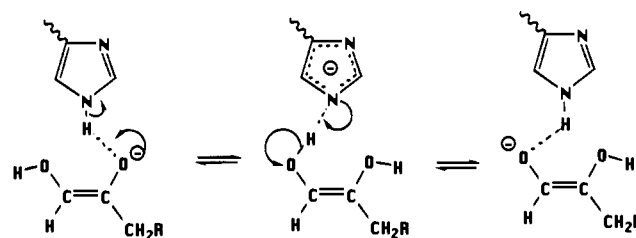


enediol or whether the intermediate remains in the enediolate form, as suggested in Scheme 1. Nickbarg et al.⁴ and Komives et al.,⁵ upon mutating His 95 to Asn or Gln, found a loss in catalytic activity of nearly 200, thus supporting the unique role of His 95. An analysis of isotopic substitution mechanistic studies also supported the interpretation of a “two-proton” mechanism in native TIM.⁶

On the other hand, we have carried out a number of theoretical calculations^{3,7} that bear on this point. Over ten years ago, we predicted that the Gln 95 mutant might lose activity not because of its different acid–base properties than His 95 but because of its difference in structure. During molecular mechanics minimization of a truncated model of the TIM active site, His 95 remained near its X-ray determined position, whereas Gln 95 moved to hydrogen bond with Glu 165.³ This interaction, supported by the subsequent crystallographic study of Gln 95 mutant,⁵ could rationalize the lower activity of a Gln 95 mutant in two ways: first, Gln 95 could inhibit the action of Glu 165 as the catalytic base, and second, Gln 95 would not be in position to provide a key element of the stabilizing positive electrostatic potential at the incipient enediolate.

In another set of calculations⁷ we showed how, at least in principle, a +1 charged placed 2.85 Å from O₂ of DHAP (along the O₂ lone pair) could stabilize proton abstraction by Glu, changing a process that was 20 kcal/mol uphill to one that was energetically “neutral” and also involved a low proton transfer energy barrier that was consistent with the rapid reaction in TIM.⁸ To be sure, this is a very simple “gas phase” model, and a more complete representation of the enzyme active site and solution environment is required to further establish its connection with reality, but it is supportive of the idea that the enzyme could provide an environment to stabilize the enediolate

Scheme 2



long enough to allow back transfer of the proton from Glu 165 to C₂ to form GAP, without invoking anything more than an “electrostatic” role of His 95.

A key element in the above “mechanism” is that the hydroxyl proton on O₁, the enediolate of DHAP (displayed in Scheme 1, step IV), be able to move readily to O₂, enabling proton delivery to C₂ rather than back to C₁. We addressed this in our previous study,³ but with a very simple model of DHAP lacking the phosphate group. Also, the level of quantum mechanical calculations in that previous study involved a lower level of accuracy than is now possible. Thus, the first focus of this paper is to study the internal proton transfer in the full DHAP enediolate model using *ab initio* calculations with a 6-31+G* basis set at the SCF and MP2 levels of theory. We are able to show that this barrier is surprisingly small, only ~2 kcal/mol at the highest level examined with local minima for both O₁ and O₂ protonated structures.

Bash, Field, Davenport, Petsko, Ringe, and Karplus⁹ examined the proposed mechanism of Knowles et al.^{5,6} using a combined semi-empirical/molecular dynamics model and supported the feasibility of His 95 to function as a Lewis acid and become an imidazolite (Scheme 2).

Since the results in ref 9, in our opinion, do not give a clear-cut answer for the relative energies of imidazole/enediolate and enediol/imidazolite (0.0 and 2.3 kcal/mol at the SCF and MP2¹¹ levels, respectively, see Table 1 in ref 9), we tried to assess

(4) Nickbarg, E. B.; Davenport, R. C.; Petsko, G. A.; Knowles, J. R. *Biochemistry* **1988**, *27*, 5948.

(5) Komives, E. A.; Chang, L. C.; Lolis, E.; Tilton, R. F.; Petsko, G. A.; Knowles, J. R. *Biochemistry* **1991**, *30*, 3011.

(6) Raines, R. T.; Straus, D. R.; Gilbert, W.; Knowles, J. R. *Philos. Trans. R. Soc. London, A* **1986**, *317*, 371.

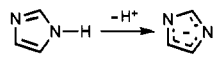
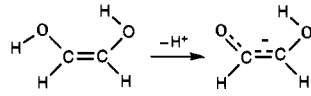
(7) Alagona, G.; Ghio, C.; Kollman, P. A. *J. Mol. Biol.* **1986**, *191*, 23.

(8) Joseph-McCarthy, D.; Lolis, E.; Komives, E. A.; Petsko, G. A. *Biochemistry* **1994**, *33*, 2815.

(9) Bash, P. A.; Field, M. J.; Davenport, R. C.; Petsko, G. A.; Ringe, D.; Karplus, M. *Biochemistry* **1991**, *30*, 5826.

(10) (a) Rieder, S. V.; Rose, I. A. *J. Biol. Chem.* **1959**, *234*, 10007. (b) Rose, I. A. *Brookhaven Symp. Biol.* **1962**, *15*, 293.

Table 1 Deprotonation Energies (kcal/mol) in Vacuo and in Aqueous Solution for Imidazole and Enediol as Models of Histidine and Enediol Phosphate (Acetic Acid Is Reported for Comparison)

system	6-31+G*// 6-31+G*		3-21+G// 3-21+G	
	in vacuo	$\epsilon = 78.5$	in vacuo	$\epsilon = 78.5$
	360.37	302.75	362.99	306.24
acetic acid \rightarrow acetate	356.45	289.58	349.91	283.29
	364.32	301.26	359.49	294.82

whether environmental effects might produce a more definite shift in the relative deprotonation energies of these molecules. Although the quantum mechanical calculations in vacuo are not relevant to solution pK_a values, quantum mechanical calculations with a continuum reaction field term¹² should give a reasonable estimate of relative pK_a values in solution. We thus compared in vacuo to continuum solvation calculations,¹² in order to evaluate the effect of an external field on the deprotonation energies of enediol and imidazole, and the results are reported in Table 1. As one can see, at the 6-31+G* level, the relative free energies in solution (with the reaction field model) are in reasonable agreement with the fact that the pK_a 's for imidazole and enediol are ~ 14 and ~ 10 .^{13,14} Using a pK_a for acetic acid of 4, the 6-31+G* solvation model predicts pK_a 's of ~ 12 and ~ 13 . At the 3-21+G level, using a pK_a of 4 for acetic acid, the calculated pK_a of imidazole is ~ 20 and that of enediol ~ 12 . Thus, the latter model significantly underestimates the stability of imidazolate.

Examining the reaction described in Scheme 2, however, one expects that proton transfer between imidazole and the enediolate will require some geometrical readjustment in the enediol to occur.

Given these uncertainties and the improvement in technology allowing a more accurate study of step IV in Scheme 1, we decided to study both it and the imidazole/enediolate proton transfer. We thus decided to revisit the fourth step of the mechanism, using the 6-31+G* basis set (the anion requests at least a set of diffuse functions) and a full geometry optimization at the SCF level, when possible. The intermolecular proton transfer proposed by Bash et al. has also been studied, considering a few geometries of the partners. Because of the size of this complex (Scheme 2), we had to use the 3-21+G basis set to study it.

Computational Details

The in vacuo and partial charge calculations were carried out using Gaussian 90¹⁵ (FPS version at UCSF and SGI version at ICQEM) and MONSTERGAUSS¹⁶ for the continuum solvent calculations.¹⁷ The MP2 calculations in solution were carried out with a modified version^{18a,b} of Hondo8.^{18c} The potential energy hypersurfaces were drawn with SURFER.¹⁹ The molecular mechanics simulations were carried out with AMBER 4.0²⁰ on the HP cluster at UCSF and the results were visualized both at ICQEM and UCSF on the E&S PS330

(11) (a) Møller, C.; Plesset, M. S. *Phys. Rev.* **1934**, *46*, 618. (b) Pople, J. A.; Binkley, J. S.; Seeger, R. *Int. J. Quantum Chem. Symp.* **1976**, *10*, 1.

(12) (a) Miertus, S.; Scrocco, E.; Tomasi, J. *Chem. Phys.* **1981**, *55*, 117. (b) Bonaccorsi, R.; Cimraglia, R.; Tomasi, J. *J. Comp. Chem.* **1983**, *4*, 567. (c) Bonaccorsi, R.; Cimraglia, R.; Tomasi, J. *Chem. Phys. Lett.* **1983**, *99*, 77. (d) Alagona, G.; Bonaccorsi, R.; Ghio, C.; Tomasi, J. *J. Mol. Struct. (Theochem)* **1986**, *135*, 39. (e) Alagona, G.; Bonaccorsi, R.; Ghio, C.; Tomasi, J. *J. Mol. Struct. (Theochem)* **1986**, *137*, 263.

(13) Chiang, Y.; Kresge, A. J. *Science* **1991**, *253*, 395.

(14) Yagil, G. *Tetrahedron* **1967**, *23*, 2855.

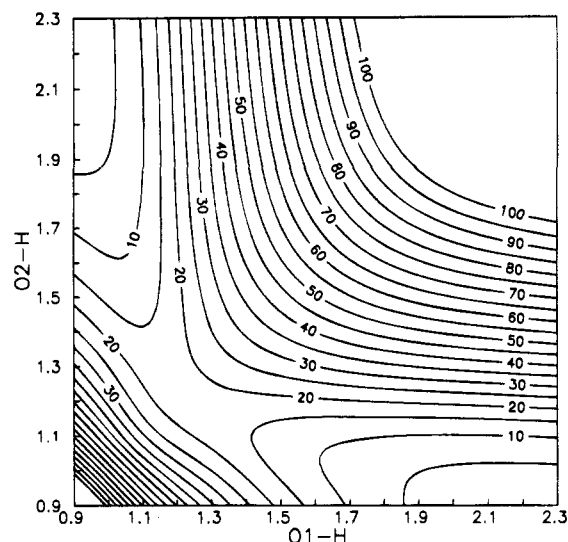
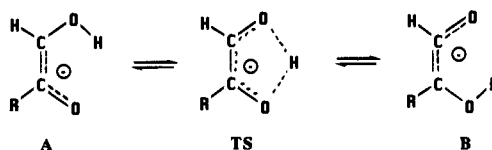


Figure 2. Potential energy surface for the intramolecular proton transfer of Scheme 3 (isopotential lines in kcal/mol, distances in Å).

Scheme 3



and SGI IRIS 4D stereographics machines, using MOGLI²¹ and MidasPlus,²² respectively.

Results and Discussion

Intramolecular Proton Transfer. In our previous study,³ we represented the enediolate of DHAP with $R = CH_3$ rather than the actual molecule $R = CH_2OPO_3^{2-}$. This was because of the computational limitations in 1984. But this was a severe approximation, since the presence of the -2 charge of the phosphate not only might change the barrier height dramatically but also might make the structure with the proton on O_2 much more stable than the one with the proton on O_1 .

We begin our calculations with the simplest model for the enediolate phosphate anion $CHO-CHOH^-$, where the reactant (A) is exactly equal to the product (B). Because of the symmetry of the system (Scheme 3), we planned to determine, in the search for the transition state (TS), the minimum energy geometries just for a few displacements of the proton along the

(15) Gaussian 90, Frish, M. J.; Head-Gordon, M.; Trucks, G. W.; Foresman, J. B.; Schlegel, H. B.; Raghavachari, K.; Robb, M. A.; Binkley, J. S.; Gonzales, C.; Defrees, D. J.; Fox, D. J.; Whiteside, R. A.; Seeger, R.; Melius, C. F.; Baker, J.; Martin, R. L.; Kahn, L. R.; Stewart, J. J. P.; Topiol, S.; Pople, J. A.; Gaussian, Inc., Pittsburgh, PA, 1990.

(16) Peterson, M. R.; Poirier, R. A. MONSTERGAUSS, Department of Chemistry, University of Toronto, Toronto, Ontario, Canada.

(17) Ghio, C. MGPIPC, ICQEM-CNR, Pisa, Italy. Revised version of MGPIPC: Bonaccorsi, R.; Cammi, R. ICQEM-CNR, Pisa, Italy.

(18) (a) Persico, M.; Cossi, M. Dipartimento di Chimica e Chimica Industriale, Università di Pisa, Pisa, Italy. (b) Cossi, M. Thesis, Università di Pisa, 1991. (c) Clementi, E., Ed. *Modern Techniques in Computational Chemistry: MOTECC-90*; ESCOM: Leiden, 1990.

(19) SURFER, Golden Software, Inc., P. O. Box 281, Golden, CO 80402.

(20) (a) Pearlman, D. A.; Case, D. A.; Caldwell, J. C.; Seibel, G. L.; Chandra Singh, U.; Weiner, P.; Kollman, P. A. (1991), AMBER 4.0, University of California, San Francisco. (b) Weiner, S. J.; Kollman, P. A.; Case, D. A.; Chandra Singh, U.; Ghio, C.; Alagona, G.; Profeta, S., Jr.; Weiner, P. *J. Am. Chem. Soc.* **1984**, *106*, 765. (c) Weiner, S. J.; Kollman, P. A.; Nguyen, D. T.; Case, D. A. *J. Comp. Chem.* **1986**, *7*, 230.

(21) MOGLI 1.1, copyright 1985, Evans & Sutherland Computer Corp.

(22) (a) MidasPlus, Computer Graphics Lab., School of Pharmacy, University of California, San Francisco. (b) Ferrin, T. E. et al. *J. Mol. Graphics* **1988**, *6*, 13.

symmetry axis, but it was a challenge to locate the TS. Several numerical troubles arose, probably linked to highly symmetric optimizations, and we had to perform the search of the whole potential energy surface, displayed in Figure 2, not only of its main diagonal. The hypersurface presents a narrow channel for the proton movement. Employing this model system and fully optimizing at the SCF/6-31+G* level, we obtain a proton transfer barrier of 19.3 kcal/mol at the SCF level, which is lowered to only 7.9 kcal/mol with the inclusion of single point MP2 correlation corrections.

In order to evaluate the effect of a polarizing field on the barrier height, we have considered the field due to a continuum dielectric medium of dielectric constant $\epsilon = 78.5$. The response of a molecule to an external field is similar in the case of fields generated either by point charges or by a solvent described within the electrostatic approximation.²³ The choice of the dielectric constant is arbitrarily set to that of water, but from our previous experience we know that the continuum effect on the energy is similar for any dielectric constant $\epsilon > 20$.²⁴ In any case, this field does not produce a significant change on the reaction: the barrier height at the SCF level (19.6 kcal/mol) is almost unaltered.

Considering the methyl-substituted enediolate ($R = \text{CH}_3$) as a model of the enediolate phosphate, the energy barriers computed from the three SCF/6-31+G* fully optimized species in which the methyl group is staggered with respect to the OH group are 19.2 and 8.2 kcal/mol at the SCF and MP2 levels, respectively. The methyl group does not affect the energy barriers, but it does affect the symmetry of the system: A is 2.0 kcal/mol more stable than B at the SCF level and just 1.5 kcal/mol more stable with the inclusion of the MP2 corrections. The situation is almost unchanged (the energy difference between A and B is 1.9 and 1.5 kcal/mol, respectively) by substituting an ethyl group for the methyl group and fully optimizing the new structures ($R = \text{CH}_2\text{CH}_3$; the methyl groups both optimize to a staggered geometry). The anion containing the slightly longer aliphatic chain shows barrier heights to the proton shuttling of 18.4 kcal/mol at the SCF level and 7.7 kcal/mol at the MP2 level.

The variation of the geometrical parameters with the substituents is limited for the species considered (A, B, TS), as can be seen by examining Tables 2–4 (supporting information). Therefore, we decided to use the geometry of ethylenediolate to model enediolate phosphate, because it was exceedingly time consuming to optimize its geometry using the 6-31+G* basis set. The internal geometry of the phosphate group was separately optimized in $\text{CH}_3\text{OPO}_3^{2-}$ at the SCF/6-31+G* level as well.

The inclusion of the phosphate group ($R = \text{CH}_2\text{-OPO}_3^{2-}$) in the model produces a dramatic effect on the barrier heights, which become 13.2 kcal/mol at the SCF level and only 2.7 kcal/mol at the MP2 level. Another interesting result is the inversion in stability between A and B: the energy of the species with the H closer to the phosphate group turns out to be more stable than A by 0.9 kcal/mol at the SCF level and by 1.5 kcal/mol at the MP2 level. The SCF energy levels for all the model compounds are reported in Figure 3a, while the corresponding MP2 levels are displayed in Figure 3b. In order to check the reliability of the model, the energies at approximately 25% and 75% of the reaction coordinate have been computed. The linear interpolation gave $R_{\text{O1-H}} = 1.091 \text{ \AA}$ and $R_{\text{O2-H}} = 1.754 \text{ \AA}$ at

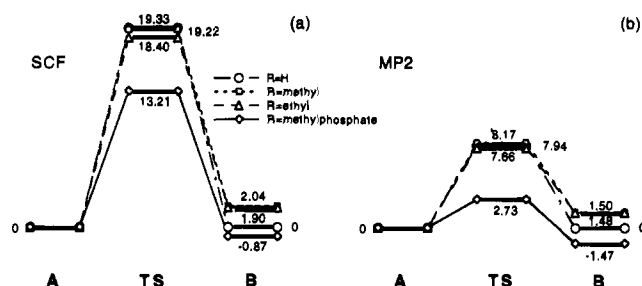


Figure 3. 6-31+G* energy levels (kcal/mol) for all the model compounds considered, $R\text{-CO-CHOH}^-$, with $R = \text{H}$, methyl, ethyl, and methyl phosphate, at the (a) SCF and (b) MP2 levels.

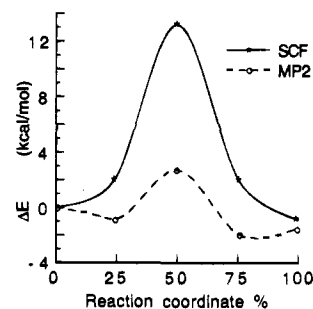


Figure 4. SCF and MP2 reaction profiles for phosphate enediolate (see text for the 25% and 75% geometries; 6-31+G* calculations).

the 25% level (and vice versa at the 75% level) but the values of $R_{\text{O1-H}} = 1.0 \text{ \AA}$ and $R_{\text{O2-H}} = 1.7 \text{ \AA}$ were representative values chosen from an inspection of the potential energy surface (Figure 2). Then all the other parameters were optimized for the simplest model ($R = \text{H}$) at the SCF/6-31+G* level, while the $-\text{CH}_2-$ geometrical parameters were interpolated between A/TS and TS/B, respectively, and the phosphate parameters were kept fixed as previously. The SCF and MP2 reaction profiles are shown in Figure 4. The two additional points are well behaved at the SCF level, but they are slightly over stabilized at the MP2 level, due to the lack of full optimization at that level. In any case, in the enediolate of DHAP and GAP it is very clear that the barrier to intramolecular proton transfer is calculated to be very small and the energies of the two proton transfer states very close in energy.

His 95 Proton Transfer. Despite the fact that intramolecular proton transfer and subsequent reprotonation of C_2 by Glu 165 appears to be the simplest way and a very low energy way to achieve isomerization catalyzed by TIM, we decided not to discard *a priori* the hypothesis of an active role of His 95 in the proton transfer, as has been postulated in ref 4–6 and studied computationally by Bash et al.⁹ (Scheme 2). As stated in the introduction, because of the size of the system, composed of enediolate ($R = \text{H}$, as a model of enediolate phosphate) and imidazole (as a model of histidine), we had to reduce the number of inner shell and valence functions in order to retain the set of sp diffuse functions, limiting ourselves to the use of the 3-21+G basis set. The complex of enediolate and imidazole involving the *anti* lone pair of O (Figure 5a, $\Delta E = -32.6 \text{ kcal/mol}$ with respect to the isolated partners) is more stable, as expected, by $\sim 12 \text{ kcal/mol}$ than that involving the *syn* O lone pair (Figure 5b, $\Delta E = -20.1 \text{ kcal/mol}$) after releasing the planarity condition. The perpendicular arrangement of the imidazole ring with respect to the enediolate plane, however, is only 0.3 kcal/mol more stable than the coplanar structure. Interestingly enough, the full geometry optimization of the adduct of Figure 5b brings the H “in” first and then moves imidazole to its *anti* location, giving the arrangement depicted in Figure 5a. This result suggested that we use the “in”-*syn* structure as an

(23) Bonaccorsi, R.; Ghio, C.; Tomasi, J. *Int. J. Quantum Chem.* **1984**, *26*, 637.

(24) Tomasi, J.; Alagona, G.; Bonaccorsi, R.; Ghio, C. In *Modelling of Structures and Properties of Molecules*; Maksic, Z., Ed.; Horwood: Chichester, 1987; p 330.

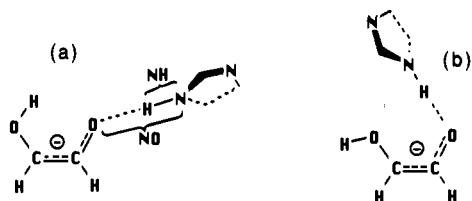


Figure 5. Intermolecular proton transfer involving His 95 (imidazole) in a perpendicular arrangement on the (a) *anti* and (b) *syn* O lone pair.

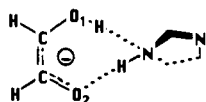


Figure 6. Schematic final structure for the 3-21+G geometry optimization carried out with the constraint $NO_1 = NO_2$.

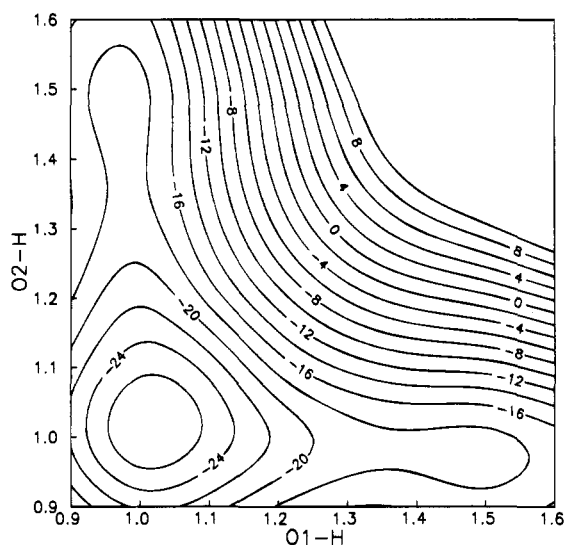


Figure 7. Potential energy surface (kcal/mol) obtained at $NO = 2.6$ Å for the variation of the O₁-H and O₂-H distances (Å) at the 3-21+G/SCF level for the adduct involving the *syn* O lone pair.

intermediate arrangement in the search for a likely reaction pathway. Therefore, a number of geometry optimizations were then carried out while keeping the imidazole ring perpendicular to the enediolate plane, at various $NO_1=NO_2=NO$ distances. With this constraint, the O₁-H and N-H bond lengths turned out to be respectively 0.957 and 1.050 Å (for $NO = 2.830$ Å, $\Delta E = -21.9$ kcal/mol (Figure 6) with one proton on enediol and one on imidazole). Applying the additional constraint O₁-H=O₂-H=OH, for OH = NO/2, with $NO = 2.4, 2.5, 2.6, 2.8$ Å, we obtain high-energy values (all above 30 kcal/mol relative to the most stable reactant complex, namely the adduct on the *anti* O lone pair of a perpendicular imidazole ring, Figure 5a). On the other hand, allowing the O₁-H=O₂-H=OH distance to relax, it turns out to be 1.02 Å for $NO = 2.6$ Å, i.e., both Hs are close to enediolate (which thus becomes an enediol) whereas imidazole is deprotonated, with an energy gain with respect to the asymmetric proton position ($\Delta E = -27.4$ kcal/mol). The tendency toward enediol and imidazolate is found also for $NO = 2.4$ Å even though it is higher in energy than with $NO = 2.6$ Å. A thorough examination of the potential energy surface (Figure 7) for the variation of O₁-H and O₂-H at $NO = 2.6$ Å led to the conclusion that there is a preferential channel for the proton transfer near the equilibrium value of O₂-H, with a barrier of about 9 kcal/mol. By examining this section of the potential energy surface for a few NO values, we find that the minimum of the maxima occurs for $NO \sim 2.62$ Å. The barrier turns out to be about 11.1 kcal/mol.

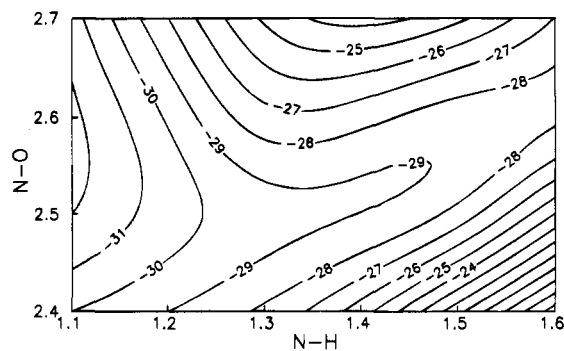
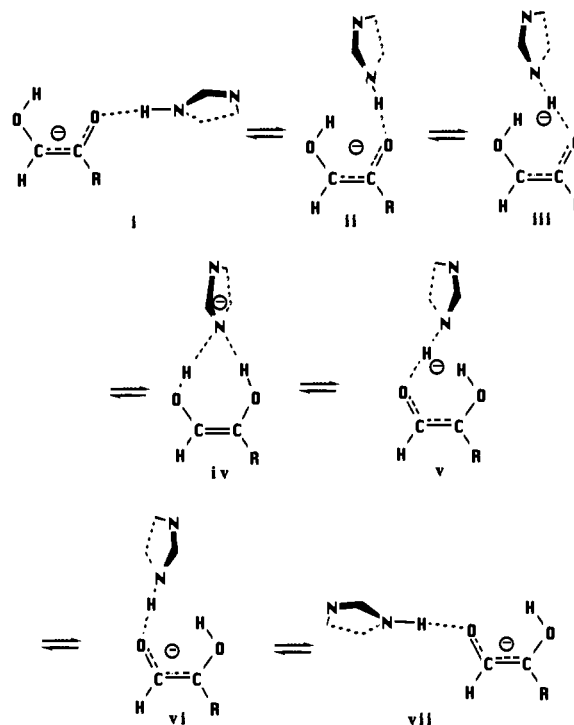


Figure 8. Potential energy surface (kcal/mol) obtained for the variation of the NO and NH distances (Å) at the 3-21+G/SCF level for the adduct involving the *anti* O lone pair.

Scheme 4

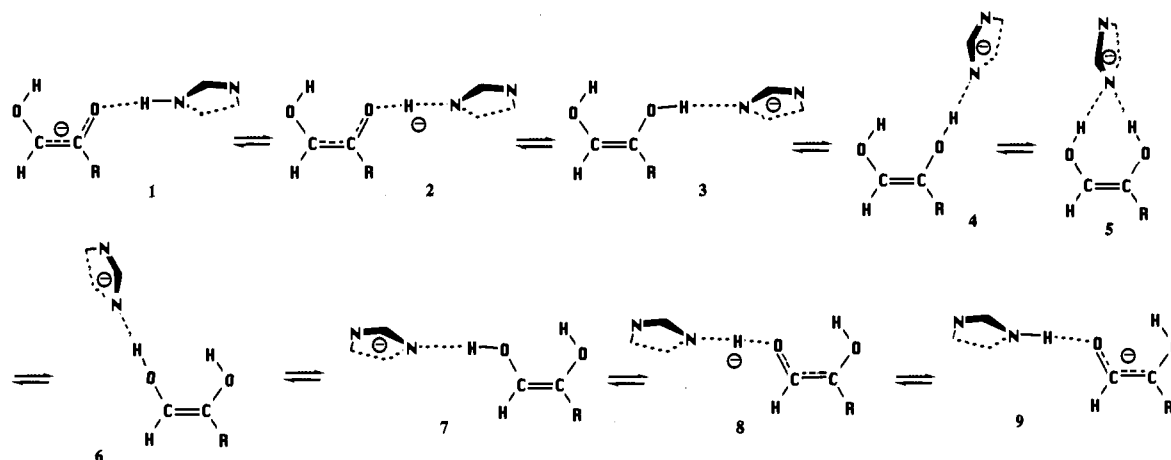


Nonetheless, these structures are all higher in energy than those obtained using the *anti* O lone pair (Figure 5a). For $NO = 2.6$ Å there is a small barrier that disappears considering the whole surface (Figure 8): the reaction pathway is uphill by about 4 kcal/mol and confirms that the preferred structure is for the proton to remain on the imidazole with no local minimum for the proton on the enediol. Thus, for the Bash et al. mechanism to occur, there must be an environmental stabilization of the imidazolate.

In summary, in order to transfer the proton from O₁ to O₂ we considered two different intermolecular mechanisms: (a) the proton transfer from imidazole to O₂ (as well as the reverse proton transfer from O₁ to imidazole) occurs when imidazole is close to the *syn* O lone pair (Scheme 4) and (b) the proton transfer, as defined above, occurs when imidazole is close to the *anti* O lone pair (Scheme 5).

With R = H, the energy profile related to the *syn* proton transfer (Figure 9a) shows a twin energy barrier (14.3 kcal/mol) of the same order of magnitude of the intramolecular proton transfer, but the mechanism involves more steps. If we suppose that the proton is released by imidazole when facing the *anti* O lone pair (b), we obtain again a twin barrier (15.1 kcal/mol) (Figure 9b), but less favorable than the previous ones

Scheme 5



and involving an even larger number of steps. Both of these barriers are significantly larger than that found for intramolecular proton transfer.

With $R = \text{CH}_2\text{OPO}_3^{2-}$, the enediol–imidazole structures are significantly stabilized (Figures 9a and 9b), as one might expect from electrostatic effects in vacuo. Nonetheless, both syn and anti proton transfer barriers are ~ 8 – 10 kcal/mol higher than the in vacuo barrier for the intramolecular mechanism. Nonetheless, it is obvious, given the large charge in this system, that we should make an effort to estimate the environmental effects on these barriers.

Environmental Effect

We have attempted to calculate the relative energies of these two mechanisms in the environment of the active site. We have carried out these calculations, using both simple enediolate ($R = \text{H}$) and full DHAP enediolate ($R = \text{CH}_2\text{OPO}_3^{2-}$) models. We do this because of the uncertainties/large errors associated with the inclusion of a localized -2 charge in these models.

His 95 Proton Shuttling. We began by docking the *ab initio* model into the enzyme active site,²⁵ twisting the enediolate with respect to the imidazole plane by 135° , to avoid any bumping of the substrate into the nearby groups. The rotation of the imidazole plane with respect to enediolate occurs with no barrier (≈ 0.3 kcal/mol), as already stated. However, the *ab initio* calculations were repeated at this reciprocal orientation to obtain reliable reference numbers.

We used models 1, 2, and 3 (Scheme 5) to represent the intermolecular transfer between His 95 and the enediolate in the active site. We began by considering the models with $R = \text{H}$. Without inclusion of environmental effects, the energies for $R = \text{H}$ (Figure 10a) are similar to those noted above, with the proton transfer $1 \rightarrow 2 \rightarrow 3$ uphill at both the SCF and MP2 levels.

A generic polarizing field, such as that produced by a continuum solvent of dielectric constant $\epsilon = 78.5$, does not change the situation. On the contrary, the starting arrangement (enediolate–imidazole, 1) is much more stabilized than the putative transition state (2, in which the H is in between enediolate and imidazole) and the enediol/imidazole complex (3), thus the rise in energy is greater than in vacuo (Figure 10b). Moreover, 3 turns out to be nearly as stable as 2.

The inclusion in the calculations of the key active site residues (Asn 11, Lys 12, Ser 96, Glu 97) via their point charge models²⁰ (after the addition of the hydrogens to the crystal structure

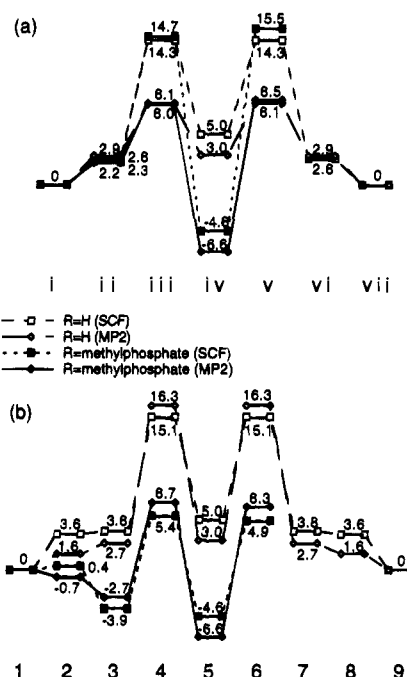


Figure 9. 3-21+G energy levels (kcal/mol) for the adducts depicted (a) in Scheme 4 and (b) in Scheme 5.

performed exploiting the edit step of AMBER²⁰ produces a sharp increase in the energy of the enediol/imidazole complex (3 = 13.3 kcal/mol with respect to 1 taken as zero, Figure 10c). When all the residues (37) within 10 Å of the substrate are included in the calculations, the energy gap between 1 and 3 is greatly reduced (Figure 10d) with 2 still along the uphill path leading to 3.

The inclusion of the phosphate in the isolated *ab initio* model produces a stabilization of 3 (-3.8 kcal/mol) greater than for 1 (after full geometry optimization at the 3-21+G/SCF level) (Figure 10a), while the barrier turns out to be only 0.4 kcal/mol at $\text{NH} = 1.2$ Å in vacuo. This is intuitively reasonable, since the presence of a -2 charge will stabilize the neutralization of the nearer enediolate, at the expense of forming an imidazole anion. However, in the presence of continuum solvent and of the enzyme field the situation changes. In the presence of the continuum solvent 3 is considerably destabilized (7.4 kcal/mol), probably because of the charge separation occurring in the system, with 2 located in the uphill path to 3 (Figure 10b). The inclusion in the calculations of the key active site residues (Figure 10c) (Asn 11, Lys 12, Ser 96, Glu 97), via their rigid point charge models, shows a trend for 2 (5.2 kcal/mol) and 3

(25) Banner, D. A.; Bloomer, A. C.; Petsko, G. A.; Phillips, D. C.; Wilson, I. A. *Biochem. Biophys. Res. Commun.* **1976**, *72*, 146.

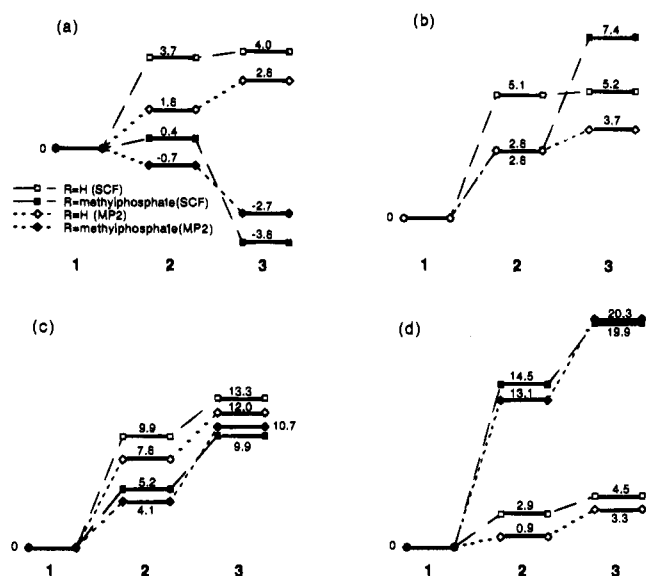


Figure 10. 3-21+G energy levels (kcal/mol) for the adducts **1** ($[\text{CHOH}-\text{RCO}] \cdots \text{imidazole}$, with the imidazole ring twisted by 135° with respect to the enediolate plane, not by 90° as in Figure 5a), **2** ($\text{CHOH}-\text{RCO} \cdots \text{H} \cdots \text{imidazole}$), and **3** ($\text{CHOH}-\text{RCOH} \cdots \text{imidazole}$) at the SCF and MP2 levels (a) in vacuo, (b) in solution (continuum solvent), and in the presence of the partial charges (c) of a few key active site residues (Asn 11, Lys 12, Ser 96, and Glu 97) and (d) of all the residues within 10 \AA of the substrate for $R = \text{H}$, and optimized with MM for $R = \text{CH}_2\text{OPO}_3^{2-}$.

(9.9 kcal/mol), analogous to that found in the continuum solvent. Considering all the residues within 10 \AA of the substrate we get high barriers for **2** both at the SCF (27 kcal/mol) and MP2 (23 kcal/mol) levels, because of the unfavorable orientation of some residues with respect to the phosphate group. Optimizing with MM simulations using AMBER [20] the positions of the 37 residues within 10 \AA of the substrate for the three geometrical arrangements of the ab initio partners, in the presence of all the outer residues kept fixed, the enzyme field changes somewhat, especially in the phosphate region, producing again an uphill, though somewhat steeper, path from **1** to **3** ($2 = 14.5$ and 13.1 kcal/mol, $3 = 19.9$ and 20.3 kcal/mol at the SCF and MP2 levels, respectively, Figure 10d).

Intramolecular Proton Transfer. For internal consistency, the 3-21+G basis set was adopted also for this mechanism. After full geometry optimization on the $R = \text{H}$ substrate, the barrier decreases with respect to that found at the 6-31+G* level by about 5 kcal/mol at the SCF level (14.7 kcal/mol) and by about 1 kcal/mol at the MP2 level (7.0 kcal/mol), due to the basis set effect (Figure 11a). The presence of the solvent does not greatly alter the barrier heights, which turn out to be 14.4 and 6.7 kcal/mol at the SCF and MP2 levels, respectively (Figure 11b).

The inclusion of the four key active site residues in the mechanism, via their partial charge description (in the same arrangement as that used for the mechanism involving His 95 and rigid for **A**, **TS**, and **B**, but including now also His 95, described through the imidazole charges), produces barriers of 12.5 and 5.2 kcal/mol besides a lack of symmetry in the system ($A \neq B$) with **B** 2.1 and 2.5 kcal/mol less favored than **A** at the SCF and MP2 levels, respectively (Figure 11c). The transition state for the proton transfer is noticeably stabilized by the correlation corrections, as expected.²⁶ The use of the partial charges of all the residues within 10 \AA of the substrate (38, including His 95, see above) leaves the barrier height almost unaltered (12.1 and 4.7 kcal/mol), while **B** is slightly more destabilized (3.7 and 3.8 kcal/mol) with respect to **A** (Figure 11d).

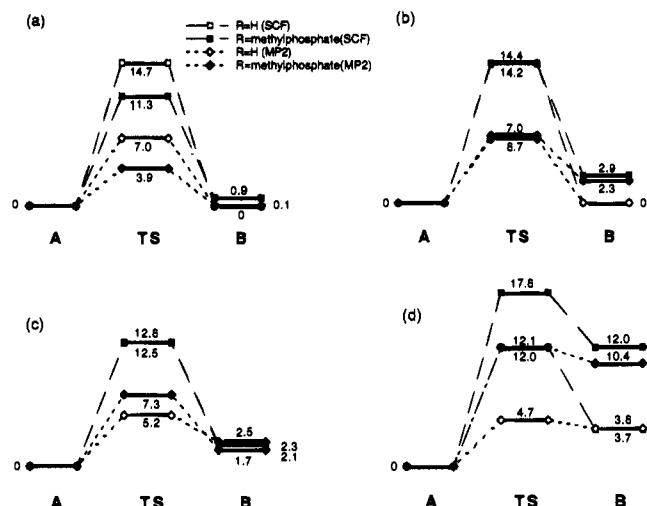


Figure 11. 3-21+G energy levels (kcal/mol) for the adducts **A** ($\text{CHOH}-\text{RCO}^-$), **TS** ($\text{CHO} \cdots \text{H}-\text{RCO}^-$), and **B** ($\text{CHO}^- - \text{RCOH}$) at the SCF and MP2 levels (a) in vacuo, (b) in solution (continuum solvent), and in the presence of the partial charges (c) of a few key active site residues (Asn 11, Lys 12, Ser 96, and Glu 97) and (d) of all the residues within 10 \AA of the substrate for $R = \text{H}$, and optimized with MM for $R = \text{CH}_2\text{OPO}_3^{2-}$.

With the addition of the phosphate group ($R = \text{CH}_2\text{OPO}_3^{2-}$), the ab initio part of the system is no longer symmetric. The in vacuo barriers are lowered both at the SCF and MP2 levels (respectively to 11.3 and 3.9 kcal/mol), whereas the energetics of the process in continuum solution (**TS** 14.2 kcal/mol, 2.9 kcal/mol (SCF); **TS** 7.0 kcal/mol, **B** 2.3 kcal/mol (MP2)) are almost unaltered with respect to those obtained for $R = \text{H}$ (Figures 11a and 11b).

The inclusion of the four key active site residues in the mechanism, as described above, produces barriers of 12.6 and 7.3 kcal/mol with **B** 2.3 and 1.7 kcal/mol less favored than **A** at the SCF and MP2 levels, respectively (Figure 11c). Because the initial model built geometry had some bad contacts, we carried out MM energy refinements for all 38 residues within 10 \AA of the substrate for its **A**, **TS**, and **B** ab initio structures, with the presence of all the remaining residues kept fixed. With this model, we obtain slightly lower barriers (17.6 and 12.0 kcal/mol), whereas **B** is more destabilized with respect to **A** (12.0 and 10.4 kcal/mol at the SCF and MP2 levels) (Figure 11d).

Mechanistic Implications and Conclusions

The most important finding here was the result, calculated at the fairly high level of ab initio electronic structure theory (6-31+G*/MP2), that the barrier to proton transfer between the O_1 and O_2 oxygens in the enediolate intermediate between DHAP and GAP is very small (≤ 5 kcal/mol) and the energy for the proton residing on O_1 is very similar to that residing on O_2 . Based on the presence of the -2 charge on the phosphate, one might have expected the proton to be highly favored on O_2 and the barrier for $O_2 \rightarrow O_1$ transfer large. Thus, our results are both surprising and gratifying. Based on the large negative charge of this molecule, one might have expected a rather small environmental effect on this transfer free energy and that is what is found with a continuum solvation model.

Komives and co-workers⁵ have proposed and Bash et al.⁹ have simulated an alternative mechanism for proton transfer between O_1 and O_2 , which requires imidazole to transfer its proton to the enediolate, making it an enediol. Unfortunately, because of computer limitations, this mechanistic possibility could be

studied only with the more limited 3-21+G basis set. In vacuo and with continuum solvent, we have shown that there is no tendency for imidazole to transfer its proton to an enediolate. When a phosphate is added to the enediolate, the transfer becomes favorable (Figure 10a), but this may be simply because any process of charge reduction (changing a -3 species into a -2 and -1 and thus delocalizing the negative charge) would be favorable in vacuo. With the addition of environmental effects, either with a continuum model (Figure 10b) or with partial charges from the enzyme active site groups (Figures 10c and 10d), the proton transfer from imidazole to enediolate becomes progressively less favorable. With the most complete active site representation (Figure 10d), this process is uphill by ~ 20 kcal/mol, with no local minimum found for proton transfer at all. However, we emphasize that our model for representing the environmental effect is not quantitatively reliable and until we use a model that can accurately calculate the pK_a 's of imidazole and enediol in solution, we cannot definitively calculate these values in the protein.

Ironically, our calculated energy difference is of the same magnitude as found by Bash et al.,⁹ who reported a local minimum ~ 12 kcal/mol higher for enediol-imidazolite than enediolate-imidazole with a barrier of ~ 16 kcal/mol to reach this state. Given that they used a different X-ray structure, force field, a less rigorous quantum mechanical model (AM1), but more extensive minimization, the qualitative agreement of the energies is, we feel, noteworthy. We should also note, based on the results reported in Table 1, that the 3-21+G basis set underestimates the stability of imidazolite by ~ 9 kcal/mol relative to experiment, so our model calculations may have well underestimated the stability of the intermolecular proton transfer mechanism.

A referee of a previous version of this paper has noted that our finding of a more stable structure for the *anti* lone pair approach of imidazole to the enediolate rather than the *syn* is inconsistent with both the X-ray structure of the hydroxamate intermediate analog²⁷ and microscopic reversibility for the proton transfer in the reverse reaction involving GAP. We do not claim to have made a definitive analysis of the intermolecular proton transfer mechanism. However, we note that our calculated barriers for both *syn* and *anti* proton transfer are similar (Figure 9) and that the calculated barrier including environmental effects is qualitatively similar to that found by Bash et al.,⁹ and both are substantially larger than that found in intramolecular proton transfer.

The Bash et al.⁹ study did not consider intramolecular proton transfer in the enediolate at all, which we find to be more energetically favorable than imidazole \rightarrow enediolate, as well as having a significant entropic advantage. A further implication of that study⁹ is that the rate limiting chemical step in TIM is the imidazole \rightarrow enediolate proton transfer. In contrast, we suggest that the initial abstraction of the C-H proton transfer by Glu 165 is rate limiting. It is hard to reconcile the mutation results for Glu 165 \rightarrow Asp 165, which lead to a $\sim 10^3$ loss in catalytic rate, with imidazole proton transfer being rate limiting. This would imply (see Bash et al.⁹ Figure 1) that replacement of Glu \rightarrow Asp would have to raise the barrier to C-H proton abstraction by ~ 9 kcal/mol (not the $\sim 3-4$ which we estimated to be reasonable⁷ in order to make that step rate limiting).

How then can one rationalize the ~ 200 -fold reduction in activity for H95Q (and H95N) TIM. As we have suggested

earlier,³ this could be simply due to the fact that Q95 and N95 are not in as good a position to stabilize the enediolate by electrostatics/H-bonding as H95 or that E165 is in a less well suited position for proton abstraction. The latter inference is supported by the crystal structure of Komives et al.⁵ Another difficulty with the suggestion that H95 is a proton donor is the fact that its pK_a (~ 14) for proton loss even considering perturbations⁵ by the enzyme environment is likely to be greater than that of Lys 13 ($pK_a \sim 9$). Given that these two groups are quite near each other in the crystal structure,²⁷ it is hard to argue that the pK_a 's would change enough to make the pK_a for H95 lower.

The implications of these calculations would be interesting to test with artificial enzymes, in which fluorinated His 95 is substituted for His 95. 2-Fluoroimidazole has a pK_a for proton loss ~ 3 pK_a units lower than that for imidazole.²⁸ Crystal structure analysis would need to be done to ascertain the structural integrity of the enzyme and it would have to be "damaged" enough to make the chemical step rate limiting, but if proton delivery from imidazole is key to catalysis, the increase in rate due to the lowered pK_a of fluorinated imidazole could be approximately equal to ΔpK_a , or about 10^3 , and likely to be significantly larger than any advantage from the more positive electrostatic potential on the His N-H due to a fluoro substitution.

The implications of our interpretation of the calculations presented here are more general than just applicable to TIM. Specifically, our interpretation of how enzymes catalyze their reactions is quite distinct from those presented by Gerlt and Gassman² and Cleland and Kreevoy.²⁹ We suggest that in most cases, enzymes need simply align and provide an appropriate electrostatic potential³⁰ to effect the catalysis they do—no pK_a balance or low barrier hydrogen bonds need be invoked. In our opinion, the interpretation presented here is simpler, requiring fewer chemical steps, and thus has an entropic advantage, as well as being favored by "Occam's razor".

Acknowledgment. P.A.K. acknowledges research support from the NIH (GM-29072) and the use of the UCSF Computer Graphics Lab. (RR-1081, T. Ferrin director).

Noted Added in Proof: R. Kluger has brought to our attention a paper [Guthrie, J. P.; Kluger, R. Electrostatic Stabilization Can Explain the Unexpected Audacity of Carbon Acids in Enzyme Catalyzed Reactions. *J. Am. Chem. Soc.* **1993**, *115*, 11569], which supports the arguments presented here for TIM. Other papers of relevance to this debate have recently appeared [Warshel, A.; Papazyan, A.; Kollman, P. A. *Science* **1995**, *269*, 102] along with rebuttals [Cleland, W.; Kreevoy, M. *Science* **1995**, *269*, 104. Frey, *Science* **1995**, *269*, 104. Scheiner, S.; Kar, T. *J. Am. Chem. Soc.* **1995**, *117*, 6970].

Supporting Information Available: Tables of reactant, product, and transition state geometries (3 pages). This material is contained in many libraries on microfiche, immediately follows this article in the microfilm version of the journal, can be ordered from the ACS, and can be downloaded from the Internet; see any current masthead page for ordering information and Internet access instructions.

JA942621W

(28) Yeh, H. J. C.; Kirk, K. L.; Cohen, L. A.; Cohen, J. S. *J. Chem. Soc., Perkin Trans. 2* **1975**, 928.

(29) Cleland, M. M.; Kreevoy, W. W. *Science* **1994**, *264*, 1887.

(30) Warshel, A. *Computer Modeling of Chemical Reactions in Enzymes and in Solution*; Wiley: New York, 1991.

(27) Davenport, R. C.; Bash, P. A.; Seaton, B. A.; Karplus, M.; Petsko, G. A.; Ringe, D. *Biochemistry* **1991**, *30*, 5821.